An Integrated and Automated Tool for Quantification of Biomechanics in Fetal and Neonatal Echocardiography

Brett A. Meyers M.S.[1], Melissa C. Brindise Ph.D.[1], R. Mark Payne M.D.[2], Pavlos P. Vlachos Ph.D.[1]

meyers18@purdue.edu, mbrindis@purdue.edu, rpayne@iu.edu, pvlachos@purdue.edu

[1] School of Mechanical Engineering, Purdue University, West Lafayette, IN, 47907

[2] Indiana University School of Medicine, Pediatrics, Pediatric Cardiology, Indianapolis, IN, 46202

Corresponding Author: Pavlos P. Vlachos, 585 Purdue Mall, West Lafayette, IN, 47907, *none*, pvlachos@purdue.edu

Total word count: 4553

This project was supported, in part, by the Indiana Clinical and Translational Sciences Institute funded, in part, by Grant Number UL1TR002529 from the National Institutes of Health, National Center for Advancing Translational Sciences, Clinical and Translational Sciences Award. The content is solely the responsibility of the authors and does not necessarily represent the official views of the National Institutes of Health. No industry partnerships collaborated on or funded this work.

Short Title:

Automated echographic biomechanics in young heart

Abstract

Objectives To show simultaneous quantification of flow and mechanics of cardiac function from fetal and neonatal echocardiograms using an integrated set of automated, physics-based, echocardiography analysis methods.

Background Quantifying ventricular biomechanics from fetal and neonatal echocardiograms presents unique and significant challenges. Existing analysis tools are designed for adults and cannot accurately assess fetal subjects.

Methods We used in-house developed analysis algorithms to quantify ventricular biomechanics from four-chamber B-mode and color Doppler routine examinations recordings for three hypoplastic left heart (HLHS) patients at 33-weeks' gestation and first week post-birth along with age-matched controls. Chamber morphology, tissue motion, atrioventricular valve inflow, global longitudinal strain, and hemodynamic flow parameters were measured.

Results Prenatal cardiac output differed between control (LV:157 ± 139 mL/min, RV:257 ± 218 mL/min) and HLHS subjects (410 ± 128 mL/min). This difference persisted for control (LV:233 ± 74 mL/min, RV:242 ± 140 mL/min) and HLHS subjects (637 ± 298 mL/min) after birth. Peak global longitudinal strain measurements did not differ *in utero* between control (LV:$12.2 \pm 4.1\%$, RV:$12.1 \pm 4.9\%$) and HLHS subjects (RV: $12.7 \pm 4.2\%$). After birth, myocardial contraction increased for the control (LV:$15.4 \pm 2.8\%$, RV:$22.9 \pm 6.9\%$) and HLHS subjects ($14.4 \pm 6.2\%$). Postnatal early filling mitral flow velocity for the control subjects (LV:58.8 ± 17.6 cm/s) and early-filling tricuspid flow of the HLHS subjects (64.8 ± 23.7cm/s) were similar, while the late filling velocity decreased for the control subject LV (33.5 ± 8.1 cm/s) compared to the HLHS subjects (66.9 ± 23.0 cm/s). Importantly, flow energy loss in the fetal HLHS hearts was increased (0.35 ± 0.19 m^3/s^2) compared to the control subjects (LV:0.09 ± 0.07 m^3/s^2, RV:0.17 ± 0.12 m^3/s^2), and further increased postnatally for the HLHS subjects (0.55 ± 0.24 m^3/s^2) compared to the control subjects (LV:0.23 ± 0.20 m^3/s^2, RV:0.09 ± 0.06 m^3/s^2).

Conclusions We demonstrate the feasibility of integrated quantitative measurements of fetal and neonatal ventricular hemodynamics and biomechanics using only four-chamber B-mode and color Doppler recordings.

Keywords: fetal ultrasound, pediatric ultrasound, image processing, strain, vector flow mapping

Short Abstract:

We integrated novel echocardiogram analysis methods to quantify ventricular flow and mechanics using apical long-axis B-mode and color Doppler imaging from fetal and neonatal subjects. Three hypoplastic left heart patients (HLHS) imaged at 33-weeks gestation and again in the first postnatal week, along with age-matched controls, were evaluated. For the first time, we show quantified hemodynamics from fetal echocardiography using flow reconstruction, flow energy loss, and intraventricular pressure, as well as global strain and strain rate. These tools are capable of longitudinal analysis of ventricle maturation, flow dynamics, and quantified measurements from routine examinations of complex congenital heart disease.

Abbreviations

AV = Atrioventricular

ALAX = Apical long axis

CHD = Congenital Heart Disease

CFI = color flow imaging

CO = Cardiac output

ECG = Electrocardiogram

EL = Energy loss

HLHS = Hypoplastic Left Heart Syndrome

GLS = Global Longitudinal Strain

GLSr = Global Longitudinal Strain Rate

LV = Left ventricle

RV = Right ventricle

VS = Vortex strength

SV = Stroke volume

ΔP = Pressure difference

Introduction

Amidst four million children born yearly in the United States, nearly 1% suffer a congenital heart defect (CHD) (1, 2), with annual treatment costs exceeding $6 billion (3) and median survival age of 1 year (4). Detecting CHDs with fetal ultrasound enables earlier care planning, improving outcomes and costs (5). Still, accurate diagnosis *in utero* remains a challenge, with top specialists detecting slightly more than 50% of CHDs (6), specialty hospitals detecting 35%, and community hospitals detecting just 13% (7).

Fetal ultrasound is mainly assessed qualitatively, with the latent ability to quantify basic cardiac biometric and function parameters (chamber dimensions, stroke volume (SV), cardiac output (CO)) (8, 9). These parameters are measured manually, producing subjective results dependent on expertise and training (8). Additionally, low image resolution, imaging depth, irregular position, heart size, and motion influence their accurate measurement (9). In cases of suspected defects and high-risk pregnancies, fetal echocardiography is used to detect CHDs (6).

Fetal echocardiography collects clinically relevant parameters, including B-mode based strain (8) and hemodynamics from pulse-wave Doppler (9). Clinical acceptance of strain measurements lags since they are vendor-specific, and frame rates and image resolution reduce accuracy. Pulse-wave Doppler does not resolve flow-induced vortices and cannot measure energy losses or pressure distributions. Advancements in 4D MRI are improving the capabilities of fetal heart assessment (10), but flow imaging has only been studied in animals to date (11). Significant motion, lack of ECG gating, and low image resolution similarly affect 4D MRI imaging. Currently, there is no integrated methodology offering the ability to jointly and comprehensively quantify chamber shape, tissue deformation, and hemodynamics from fetal scans.

This study applies an integrated and automated echocardiography analysis method for the measurement of cardiac biomechanics from fetal and neonatal echocardiograms. The analysis combines chamber and hemodynamic quantification along with global longitudinal strain (GLS) and strain rate (GLSr). The employed tools are not based on machine learning or shape models, are not vendor-specific, and do not rely on heuristics adopted from adult echocardiography. These advancements uniquely enable the adoption of these tools for routine echocardiogram analysis.

Here, we present the methodology and demonstrate its feasibility and clinical utility in a cohort of hypoplastic left heart syndrome (HLHS) subjects and age-matched controls. We quantified the biomechanics of the left (LV) and right ventricle (RV) in control subjects and compared them

against the HLHS right ventricle. The HLHS presents a demonstratively challenging clinical scenario that punctuates the robustness and capability of the proposed method.

Methods

Study population

Twelve examinations were retrospectively selected from within the Indiana University Health network. The cohort comprised three HLHS subjects and corresponding age-matched controls, with fetal exams performed at an average gestational age of 33 weeks and neonatal exams in the first week of birth. Datasets without B-mode and color flow imaging (CFI) recordings in the apical long-axis (ALAX) view were excluded. The Institutional Review Board for Human Studies for Purdue and Indiana universities approved the study.

Echocardiography

Sonographers performed fetal echocardiograms on Acuson SC200 ultrasound systems (Siemens Medical Solutions USA, Inc., Malvern, Pennsylvania) with Siemens 6C1 or 4V1 curved-array transducers. Sonographers performed neonatal echocardiograms on either iE33 (Philips, Andover, Massachusetts) or Acuson SC2000 (Siemens Medical Solutions USA, Inc., Malvern, Pennsylvania) ultrasound systems. Recordings taken on iE33 systems used S12-4 phased-array transducers, while those taken on Acuson SC200 systems used 8V3 or 10V4 phased-array transducers. American Society of Echocardiography guidelines were followed (9, 12).

Image analysis workflow

The analysis workflow, summarized in Figure 1, outputs cardiac biomechanics measurements of the LV and RV from B-mode and CFI ALAX recordings. These modalities are utilized because sonographers are well-trained in their recording, which enhances analysis consistency. The workflow automates measurements, enabling once challenging and highly user-variable analysis to become routine. All algorithms run in MATLAB (The MathWorks, Natick, Massachusetts).

Step 1: Tracking user input annulus and apex positions

One set of user inputs marking the ventricle apex and atrioventricular (AV) annulus positions on the first recorded frame, depicted in Figure 1**-1,** are required for each scan. These inputs are tracked temporally using a speckle tracking algorithm, described in Appendix A. The tracked positions provide measurements of ventricle relaxation.

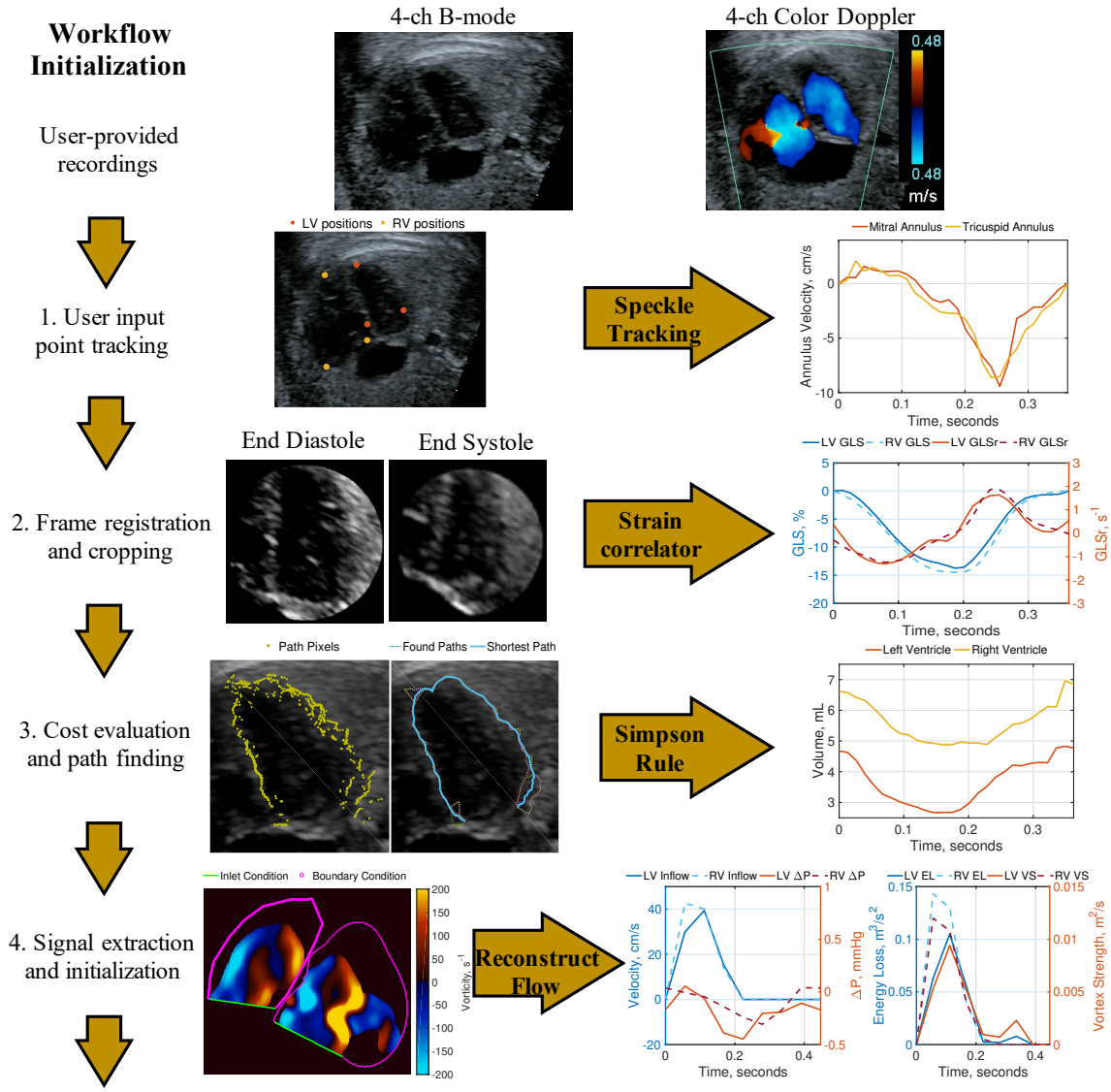

Workflow Report

Left Ventricle Function measurements

E (cm/s): 39	SV (ml): 2.0
A (cm/s): N/A	CO (ml/min): 292
EL(m^3/s^2): 0.10	$\|GLS\|_{max}$(%): -13.8
VS(m^2/s): 0.010	GLSre (s^{-1}): 1.6
ΔP(mmHg)	GLSrs (s^{-1}): -1.3
Suction: 0.06	s' (cm/s): 1.6
Recovery: -0.45	e' (cm/s): -8.6
Ejection: -0.11	a' (cm/s): N/A

Right Ventricle Function measurements

E (cm/s): 43	SV (ml): 2.0
A (cm/s): N/A	CO (ml/min): 256
EL(m^3/s^2): 0.14	$\|GLS\|_{max}$(%): -14.5
VS(m^2/s): 0.012	GLSre (s^{-1}): 1.9
ΔP(mmHg)	GLSrs (s^{-1}): -1.3
Suction: 0.04	s' (cm/s): 2.1
Recovery: -0.31	e' (cm/s): -9,4
Ejection: 0.04	a' (cm/s): N/A

Figure 1: Echocardiogram analysis workflow. Analysis begins with the user providing A4C views. (1) AV annulus and apex feature points are provided to initialize automated analysis. (2) B-mode frames are co-registered, cropped, and processed to quantify GLS. (3) B-mode frames are evaluated to find pixel costs and paths for ventricle segmentation and volume quantification. (4) Color Doppler frames are processed to extract the signal, segment the ventricle, set initial conditions, and reconstruct velocity fields. Cardiac function measurements are compiled into a workflow report.

AV annulus positions are differentiated temporally to obtain velocities and adjusted relative to the apex, which is assumed stationary during the heartbeat. Peak annulus velocities for systolic ejection (s'), early diastolic filling (e'), and late diastolic filling (a') are automatically measured. Automated speckle tracking mitral annulus position and velocity measurements has been previously validated (13).

Step 2: Global longitudinal strain

Commercial speckle tracking tools measure GLS and GLSr and have shown potential in assessing cardiac function and identifying CHDs from fetal and neonatal imaging (8, 14), but existing limitations prevent broad adoption. First, the tools require an ECG for co-registration and no excessive movement, which are impossible in fetal imaging and challenging in neonatal imaging (15). Second, ultrasound system settings must be optimized for suitable quality and frame rates (16), requiring training that is not widely available (17).

A novel algorithm is used to measure GLS and GLSr from the whole ventricle image (18), bypassing the above limitations. Briefly, the B-mode recording frames are co-registered using the tracked positions and cropped to keep the ventricle image, shown in Figure 1-**2**. A specialized correlation kernel estimates GLSr between frames and is then integrated to resolve GLS. The kernel is described in Appendix A. Peak GLS ($|GLS|, \max$), peak early diastole GLSr (GLSre), and peak systole GLSr (GLSrs) are output to quantify ventricular deformation.

Step 3: Unsupervised chamber segmentation

Chamber segmentation is uncommon in fetal echocardiography due to poor recording quality, resolution, and model assumptions (8). Even so, Simpson's rule for volume estimation from fetal imaging has shown good accuracy compared to high fidelity tools (19, 20) and is an accepted tool in neonatal imaging (21). Measurements are hand-drawn and undergo correction, which increases observer variability, user time, and requires specialized training.

The unsupervised segmentation tool (ProID) automates ventricle detection and volume estimation. The tool identifies ventricle boundaries using an iterative Dijkstra's algorithm (22), which finds the shortest path of pixels around the ventricle image, shown in Figure 1-**3**. ProID overcomes contrast-to-noise and resolution limitations that are common in natal imaging (23) by employing an echocardiogram-specific cost-matrix. The tracked positions are used to initialize ProID for each frame. Further description is provided in Appendix A. The segmentations are

processed using Simpson rule to quantify volume. End diastolic volume (EDV) and end-systolic volume (ESV) are output along with SV and CO, which quantify systolic function.

Step 4: Color Flow Imaging hemodynamics analysis

CFI is used clinically to detect septal and valve defects. Abnormal flow patterns are present in fetuses with CHDs (8), which can improve detection when using quantitative tools. Doppler vector reconstruction, or DoVeR, resolves the underlying 2D velocity vector field of blood flow within the ventricle from CFI using the relationship between blood flow rate and fluid rotation (24). DoVeR uses the tracked positions and ProID to segment the ventricle in each frame. These segmentations are used to set initial conditions for the DoVeR algorithm, shown in Figure 1**-4**. The vector fields are evaluated for peak early (E) and late (A) filling velocities, flow energy loss (EL) and vortex strength (VS) as well as the annulus-to-apex suction pressure (suction ΔP), pressure recovery (recovery ΔP), ejection pressure (ejection ΔP), and AV valve center to minimum pressure (AV-to-P_{min}) distance from computed pressure fields. Further description of DoVeR and pressure field reconstruction are provided in Appendix A.

Statistical Analysis

Data are reported as mean$\pm$SD. We compared each parameter across conditions and ages using the paired Student's T-test. A two-tailed p-value < 0.05 was considered statistically significant. We performed statistical analysis using the MATLAB Statistics toolbox.

Results

Visualization and subject characterization

Figure 2 displays single beat ventricle volumes and strain from a control fetal subject, a control neonatal subject, and one HLHS subject from their fetal and neonatal echocardiograms. The control LV and RV are shown in blue and red, respectively. The HLHS RV is shown in purple.

In control subjects, the ventricles shorten from end diastole (Figure 2a-1 and 2b-1) to end systole (Figure 2a-2 and 2b-2) as the AV annulus moves, ejecting blood during systole. Fetal EDV (RV: 2.99 mL, LV: 2.75 mL) and SV (RV: 0.80 mL, LV: 1.11 mL) are similar (Figure 2a-3), while RV peak GLS exceeded LV peak GLS (RV: -18.73%, LV: -14.81%; Figure 2a-4). Neonatal EDV (RV: 5.94 mL, LV: 5.71 mL; Figure 2b-3), SV (RV: 2.50 mL, LV: 2.55 mL), and peak GLS (RV: -14.38%, LV:-14.10%; Figure 2b-4) measurements between ventricles were similar.

For the HLHS subject, the RV (Figure 2c-1 and 2d-1) occupies the region of both ventricles in controls. This morphology change produces a volume increase compared to the normal RV and allows for changes in hemodynamics. The fetal echocardiogram SV was 2.72 mL (Figure 2c-3), which increased to 3.61 mL (Figure 2d-3) by the neonatal exam. Fetal and neonatal RV peak GLS were -7.72% and -8.83%, respectively. This subject's strain was lower compared to the controls.

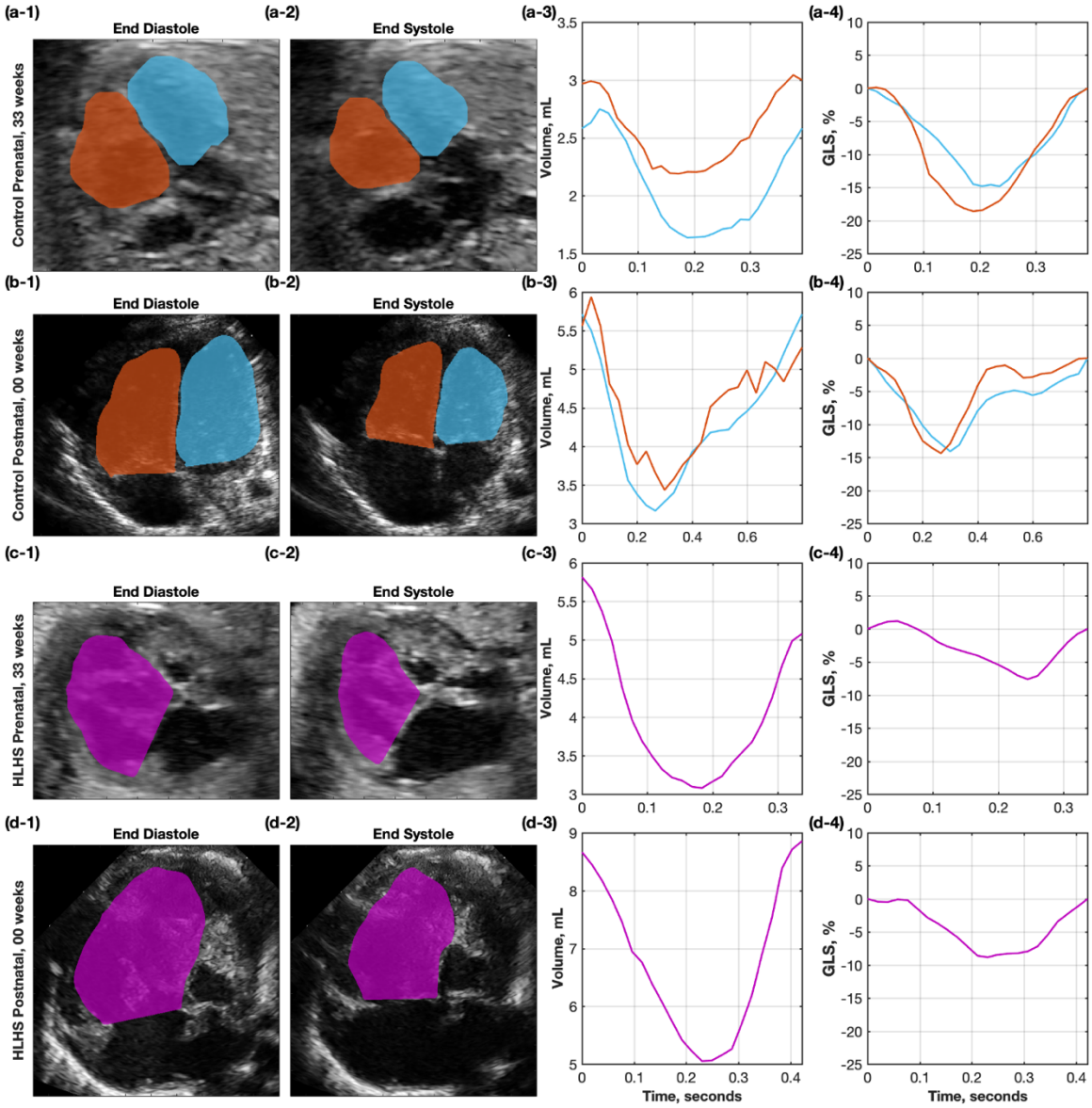

Figure 2: Ventricle volumes (1-3) and strain (4) measured from the LV and RV of a normal (a) fetal heart and a (b) neonatal heart as well as the RV from an HLHS patient from a (c) fetal heart exam and (d) neonatal heart exam.

Figure 3 shows single beat flow reconstruction vector fields overlaid onto EL and pressure field reconstructions with closed contours of identified vortices. Results are presented for a fetal control

subject, a neonatal control subject, and one HLHS subject from their fetal and neonatal echocardiograms. Frames at diastolic filling and systolic ejection are provided.

Diastolic filling occurs when blood flows into the ventricles through the AV valves, forming a shear region with increased EL and a vortex pair. The fetal LV (Figure 3a-1, right) EL is lower compared to the RV (left), while vortex pairs are present in both ventricles (Figure 3c-1). The neonate (Figure 3a-3) shows similar EL characteristics to the fetal subject with no distinct vortex pairs (Figure 3c-3). The fetal HLHS RV (Figure 3b-1) EL is elevated compared to the control RV with a vortex pair (Figure 3d-1). The neonatal HLHS RV (Figure 3b-3) EL is elevated and a vortex pair present (Figure 3d-3) with smaller energy-inefficient vortices.

Systolic ejection occurs when blood flows from the ventricle through the outflow tract. The fetal RV (Figure 3a-2, left) and neonatal RV (Figure 3a-4, left) show elevated EL along the outflow compared to the LV outflow. Both the HLHS fetal RV (Figure 3b-2) and neonatal RV (Figure 3b-4) outflow tracts are out of view.

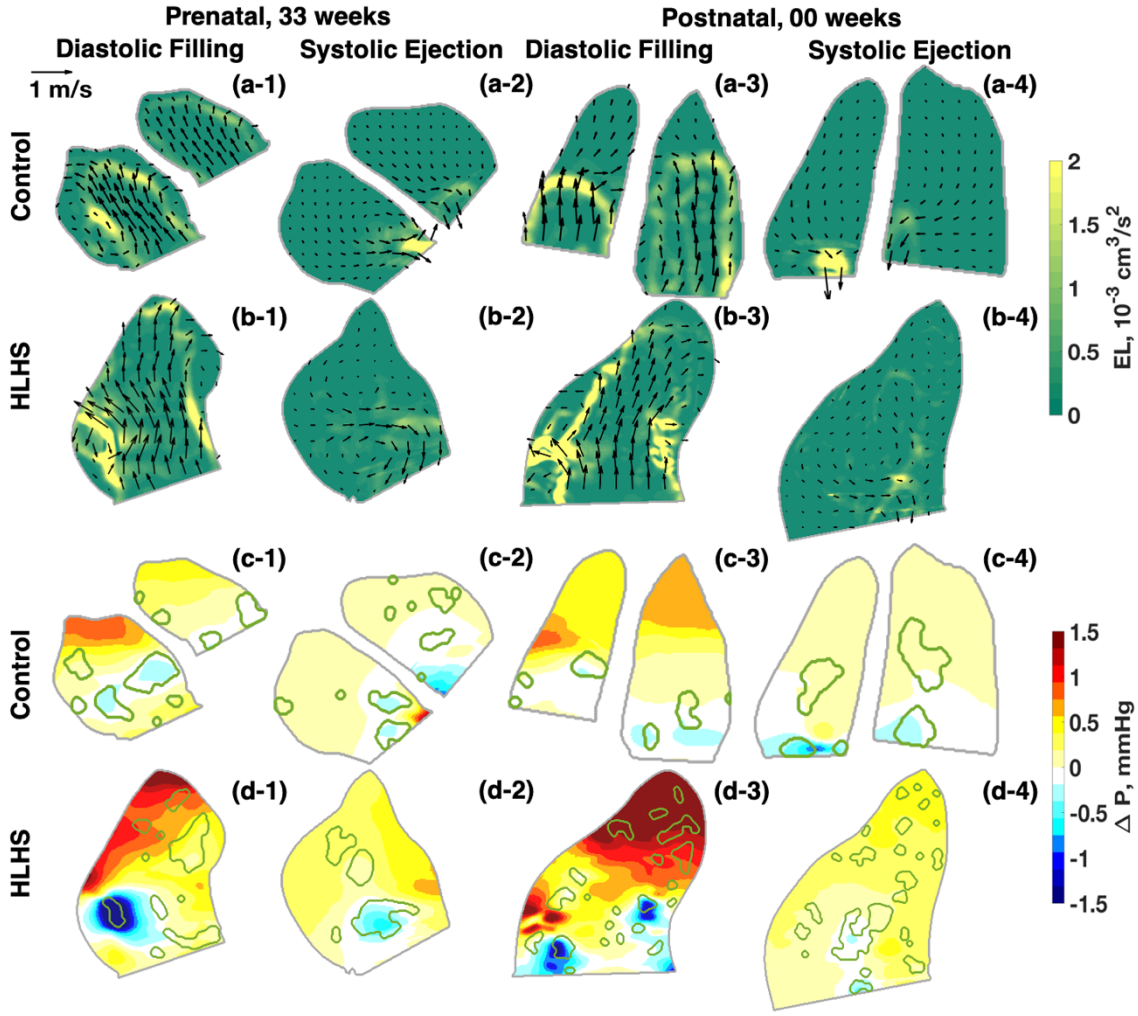

Figure 3: Vector reconstruction of flow in the LV and RV of a healthy (a-1,2) fetal heart and (a-3,4) neonatal heart and flow in the RV of an HLHS subject from a (b-1,2) fetal exam and a (b-3,4) neonatal heart exam during diastolic filling and systolic ejection. Vectors are overlaid onto energy loss estimates. Pressure reconstructions are provided for the (c) healthy and (d) HLHS subjects. Closed contours (green) correspond to vortices.

Statistical Analysis

Systolic function.

Measured parameters for the control and HLHS hearts are provided in Figure 4. We observed increased SV in fetal HLHS subjects (2.40 ± 0.71 mL) compared against the control LV (0.97 ± 0.81 mL) and RV (1.72 ± 1.37 mL). This continued after birth, with neonatal HLHS SV (4.50 ± 2.32 mL) doubling the control LV (2.37 ± 0.91 mL) and RV (2.45 ± 1.45 mL). Fetal HLHS subject CO (410 ± 128 mL/min) was elevated compared to the control LV (157 ± 139 mL/min) and RV (257 ± 218 mL/min). Similarly, neonatal HLHS subject CO (637 ± 298 mL/min)

remained elevated compared to the control LV (233 ± 74mL/min) and RV (242 ± 140 mL/min). The metrics indicate the HLHS heart adapts *in utero* to accommodate added blood volume.

Peak s' velocities in fetal HLHS subjects (2.86 ± 1.10 cm/s) were elevated compared to the control LV (2.72 ± 0.62 cm/s) and RV (2.21 ± 1.00 cm/s). Neonatal peak s' velocities were elevated in HLHS subjects (3.05 ± 0.93 cm/s) compared to the control LV (2.14 ± 0.61 cm/s) but not the RV (3.19 ± 1.02 cm/s). Peak GLS in the fetal cases were similar across HLHS ($12.7 \pm 4.2\%$), control LV ($12.2 \pm 4.1\%$), and control RV ($12.1 \pm 4.9\%$) measurements. Neonatal HLHS peak GLS ($14.4 \pm 6.2\%$) was similar to the control LV ($15.4 \pm 2.8\%$), while the control RV ($22.9 \pm 6.9\%$) significantly increased. Peak GLSrs in the fetal cases were similar across HLHS (1.37 ± 0.61 s^{-1}), control LV (1.11 ± 0.31 s^{-1}), and control RV (1.23 ± 0.54 s^{-1}) measurements. Neonatal peak GLSrs was similar across HLHS (1.34 ± 0.51 s^{-1}), control LV (1.24 ± 0.32 s^{-1}), and control RV (1.66 ± 0.33 s^{-1}) measurements. Finally, the fetal ejection pressure difference was elevated in the HLHS subjects (-0.94 ± 0.71 mmHg) compared to the control LV (-0.48 ± 0.31 mmHg) and RV (-0.54 ± 0.44 mmHg). The neonatal control ejection pressure difference increases for both the LV (-0.76 ± 0.34 mmHg) and RV (-0.74 ± 0.28 mmHg) while the neonatal HLHS (-0.61 ± 0.80 mmHg) measurements do not change significantly. These metrics indicate that the HLHS right heart increases annular plane motion to efficiently eject blood *in utero*, overcoming the volume overload and increased vascular resistance, which induced the reduced myocardial contraction.

Diastolic function.

Increased e' velocity was observed in fetal HLHS subjects (1.88 ± 0.97 cm/s) as compared against the control LV (1.23 ± 0.81 cm/s) and RV (1.19 ± 0.57 cm/s). After birth, peak e' velocity for the control RV (1.80 ± 0.73 cm/s) increases compared to HLHS (1.18 ± 1.12 cm/s) and control LV (1.26 ± 0.50 cm/s) measurements. We observed peak a' velocities in fetal HLHS (0.84 ± 0.98 cm/s), control LV (1.08 ± 0.80 cm/s), and control RV (0.85 ± 0.82 cm/s) measurements were similar. Neonatal HLHS peak a' velocity (1.36 ± 0.57 cm/s) becomes elevated compared to control LV (0.88 ± 0.40 cm/s) and control RV (1.17 ± 0.74 cm/s). The fetal HLHS peak GLSre (1.87 ± 0.95 s^{-1}) was elevated compared to the control LV (1.24 ± 0.80 s^{-1}) and control RV (1.23 ± 0.61 s^{-1}). Neonatal control LV peak GLSre measurements (1.21 ± 0.50 s^{-1}) remain unchanged while HLHS peak GLSRe (1.10 ± 1.09 s^{-1}) decreases and control RV (1.70 ± 0.71 s^{-1}) increases. These metrics indicate that the heart adapts to efficiently relax but

annular motion increases in late diastole to fill the HLHS right heart in the presence of reduced compliance.

Peak E velocity in the fetal HLHS subjects (44.5 ± 20.2 cm/s) was elevated compared to the fetal control LV (25.5 ± 13.2 cm/s) and RV (30.5 ± 20.8 cm/s). Neonatal control LV peak E velocity increases significantly (58.8 ± 17.6 cm/s) compared to HLHS (64.8 ± 23.7 cm/s) and control RV (44.4 ± 13.7 cm/s) measurements. Peak A velocity in the fetal HLHS subjects (43.7 ± 12.1 cm/s) was similar to the control LV (36.9 ± 12.8cm/s) and RV (37.3 ± 11.3 cm/s). After birth elevated peak A velocity was observed in the HLHS subjects (66.9 ± 23.0 cm/s) compared to the control LV (33.5 ± 8.1 cm/s) and RV (46.0 ± 6.7 cm/s). These metrics indicate the HLHS right heart requires increased atrial contraction to fill the ventricle.

Suction ΔP was as similar across fetal HLHS (0.31 ± 0.34 mmHg), control LV (0.19 ± 0.16 cm/s), and control RV (0.24 ± 0.36 cm/s) measurements. Neonatal HLHS suction ΔP significantly increases (1.26 ± 1.57 mmHg) compared to the control LV (0.27 ± 0.18 mmHg) and RV (0.56 ± 1.11 mmHg). Recovery ΔP was elevated in fetal HLHS subjects (-1.78 ± 0.64 mmHg) compared to the control LV (-0.71 ± 0.29 mmHg) and RV (-0.97 ± 0.55 mmHg). Recovery ΔP increases for neonatal HLHS (-1.97 ± 1.35 mmHg), control LV (-1.72 ± 1.41 mmHg) and control RV (-1.59 ± 1.46 mmHg) measurements. AV-to-P_{min} occurs further from the annular plane for the fetal HLHS right heart (7.4 ± 3.0 mm) compared to the control LV (5.4 ± 2.7 mm) and RV (6.1 ± 2.3 mm). This is maintained for the neonatal HLHS (10.5 ± 5.1 mm), control LV (3.7 ± 2.6 mm), and control RV (4.8 ± 2.8 mm). These metrics indicate that the HLHS right heart experiences greater pressure differences to achieve efficient filling.

Peak EL in fetal HLHS subjects (0.35 ± 0.19 m^3/s^2) was elevated compared to the control LV (0.09 ± 0.07 m^3/s^2) and RV (0.17 ± 0.12 m^3/s^2). Neonatal HLHS (0.55 ± 0.24 m^3/s^2) and control LV (0.23 ± 0.20 m^3/s^2) peak EL increases while the control RV (0.09 ± 0.06 m^3/s^2) is reduced. Peak VS in fetal HLHS subjects (225 ± 73 cm^2/s) was elevated compared to the control LV (77 ± 38 cm^2/s) and RV (113 ± 52 cm^2/s). Neonatal HLHS (345 ± 74 cm^2/s) and control LV (137 ± 83 cm^2/s) peak VS increases while the control RV (71 ± 32 cm^2/s) is reduced. These metrics indicate that the increased HLHS right heart area causes greater energy loss, reducing efficient redirection of the blood volume before systolic ejection.

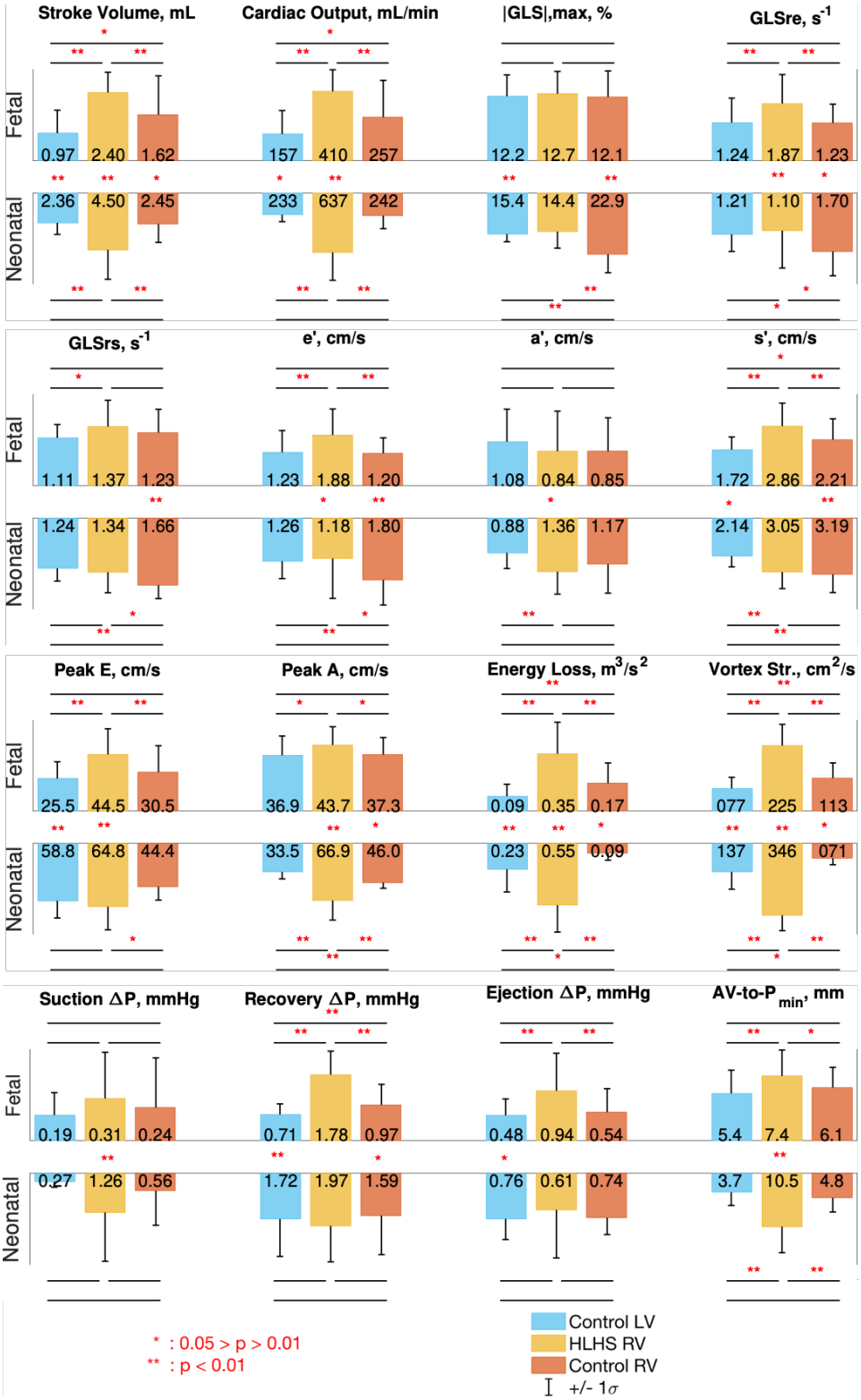

Figure 4: Measurements from fetal and neonatal scans used to assess ventricular function in healthy and HLHS patients. The p-values provided are between healthy left and right ventricle measurements and between each healthy ventricle and HLHS right ventricles, along with p-values across the prenatal and postnatal age groups for both conditions.

Discussion

This study quantified the biomechanics of ventricular function for normal and HLHS hearts from fetal and neonatal echocardiograms using new automated analysis methods. Our findings indicate that aside from typical HLHS RV remodeling, altered diastolic blood flow and reduced compliance occur. This is only realized with the integrated platform which assesses ventricular chamber morphology, deformation, and hemodynamics.

HLHS defects are readily identified with fetal ultrasound when the RV remodels to support the pulmonary and systemic circulations. While SV and CO differed significantly ($p < 0.05$) between control and HLHS subjects, total SV between the fetal HLHS (2.40 mL) and control (2.59 mL) hearts, and between the neonatal HLHS (4.50 mL) and control (4.81 mL) hearts closely matched. These parameters enumerate remodeling but are readily observable by qualitative assessment.

While the fetal HLHS RV deforms like the controls based on GLS, GLSrs ($p < 0.05$) and s' ($p < 0.01$) increase to produce this effect. The HLHS RV shows reduced deformation after birth, but GLSrs and s' were unchanged, indicating reduced compliance and increased stiffness. This is only found with speckle tracking and strain measurements, which are just seeing clinical acceptance.

Reduced compliance is observable through the elevated pressure differences required to fill and empty the HLHS RV, which also contributes to the altered flow patterns. In the fetal condition, increased recovery and ejection pressure differences are present for the HLHS RV ($p < 0.01$), which indicate added resistances. These differences diminish after birth, although suction and recovery pressure differences remain elevated. The accompanying altered flow patterns for the HLHS RV are the most sensitive, showing elevated energy loss and vortex strength in both fetal and neonatal conditions ($p < 0.01$), indicating the formation of large, energy-inefficient vortices. This work shows the first such application of CFI-based flow reconstruction using fetal imaging, offering new metrics for early detection of cardiac anomalies and possibly altering the treatment course of the infant. Importantly, these new indices will allow better quantification of myocardial performance thus improving the diagnosis and management of fetal heart failure.

Study Limitations

We treat each heartbeat as an independent observation, which potentially introduces bias into the reported means. Our cohort comprised 12 studies across 9 subjects, so investigating functional differences between conditions may not be sufficiently supported. Additional fetal and pediatric measurements would enable further quantification of functional differences.

Conclusions

A new set of integrated, automated, vendor agnostic echocardiogram analysis methods is introduced for evaluating cardiac biomechanics from fetal and neonatal scans. This workflow enables clinically relevant measurements to be obtained more readily from a single scan, saving time, and reducing the need for specialized training. Importantly, no modification of image acquisition or scan technique was required to obtain these data. Our evaluation of HLHS and normal subjects supports the capabilities of our methods to provide reliable measurement from demonstratively challenging echocardiograms. Altered morphology, hemodynamics, and ventricular relaxation were observed in the presence of a severe CHD, indicating the methods can potentially provide earlier detection of anomalies *in utero* and may lead to improving treatment practices *ex utero*.

References

1. Hamilton BE, Osterman MJK, Driscoll AK, et al. Births: Provisional data for 2017. NVSS Vital Stat. Rapid Release 2018;2:1–21.

2. Benjamin EJ, Virani SS, Callaway CW, et al. Heart disease and stroke statistics—2018 update: a report from the American Heart Association. Circulation 2018;137:e67–e492.

3. Arth AC, Tinker SC, Simeone RM, Ailes EC, Cragan JD, Grosse SD. Inpatient hospitalization costs associated with birth defects among persons of all ages—United States, 2013. MMWR. Morb. Mortal. Wkly. Rep. 2017;66:41.

4. Gilboa SM, Salemi JL, Nembhard WN, Fixler DE, Correa A. Mortality resulting from congenital heart disease among children and adults in the United States, 1999 to 2006. Circulation 2010;122:2254–2263.

5. Tworetzky W, McElhinney DB, Reddy VM, Brook MM, Hanley FL, Silverman. NH. Improved Surgical Outcome After Fetal Diagnosis of Hypoplastic Left Heart Syndrome. Circulation 2001;103:1269–1273.

6. Huhta JC, Paul JJ. Doppler in fetal heart failure. Clin. Obstet. Gynecol. 2010;53:915–929.

7. Todros T, Capuzzo E, Gaglioti P. Prenatal diagnosis of congenital anomalies. Images Paediatr. Cardiol. 2001;3:3.

8. Donofrio MT, Moon-Grady AJ, Hornberger LK, et al. Diagnosis and treatment of fetal cardiac disease: a scientific statement from the American Heart Association. Circulation

2014;129:2183–2242.

9. Rychik J, Ayres N, Cuneo B, et al. American society of echocardiography guidelines and standards for performance of the fetal echocardiogram. J. Am. Soc. Echocardiogr. 2004;17:803–810.

10. Marini D, van Amerom J, Saini BS, Sun L, Seed M. MR imaging of the fetal heart. J. Magn. Reson. Imaging 2020;51:1030–1044.

11. Schrauben EM, Saini BS, Darby JRT, et al. Fetal hemodynamics and cardiac streaming assessed by 4D flow cardiovascular magnetic resonance in fetal sheep. J. Cardiovasc. Magn. Reson. 2019;21:8.

12. Lai WW, Geva T, Shirali GS, et al. Guidelines and Standards for Performance of a Pediatric Echocardiogram: A Report from the Task Force of the Pediatric Council of the American Society of Echocardiography. J. Am. Soc. Echocardiogr. 2006;19:1413–1430.

13. Haruki N, Takeuchi M, Gerard O, et al. Accuracy of measuring mitral annular velocity by 2D speckle tracking imaging. J. Cardiol. 2009;53:188–195.

14. Colquitt JL, Pignatelli RH. Strain imaging: the emergence of speckle tracking echocardiography into clinical pediatric cardiology. Congenit. Heart Dis. 2016;11:199–207.

15. Germanakis I, Gardiner H. Assessment of fetal myocardial deformation using speckle tracking techniques. Fetal Diagn. Ther. 2012;32:39–46.

16. Matsui H, Germanakis I, Kulinskaya E, Gardiner HM. Temporal and spatial performance of vector velocity imaging in the human fetal heart. Ultrasound Obstet. Gynecol. 2011;37:150–157.

17. Bahtiyar MO, Copel JA. Improving detection of fetal cardiac anomalies: a fetal echocardiogram for every fetus? J. ultrasound Med. 2007;26:1639–1641.

18. Meyers BA, Brindise MC, Jani V, Kutty S, Vlachos PP. Direct estimation of global longitudinal strain from echocardiograms using a logarithm-scaled Fourier magnitude correlation. arXiv Prepr. arXiv2003.11672 2020.

19. Schoonderwaldt EM, Groenenberg IALL, Hop WCJJ, Wladimiroff JW, Steegers EAPP. Reproducibility of echocardiographic measurements of human fetal left ventricular volumes and ejection fractions using four-dimensional ultrasound with the spatio-temporal image correlation modality. Eur. J. Obstet. Gynecol. Reprod. Biol. 2012;160:22–29.

20. DeVore GR, Klas B, Satou G, Sklansky M. Evaluation of Fetal Left Ventricular Size and

Function Using Speckle-Tracking and the Simpson Rule. J. Ultrasound Med. 2019;38:1209–1221.

21. Lopez L, Colan SD, Frommelt PC, et al. Recommendations for quantification methods during the performance of a pediatric echocardiogram: a report from the Pediatric Measurements Writing Group of the American Society of Echocardiography Pediatric and Congenital Heart Disease Council. J. Am. Soc. Echocardiogr. 2010;23:465–495.

22. Dijkstra EW. A note on two problems in connexion with graphs. Numer. Math. 1959;1:269–271.

23. Donofrio MT, Moon-grady AJ, Hornberger LK, et al. Diagnosis and Treatment of Fetal Cardiac Disease. Circulation 2014;129:2183–2242.

24. Meyers BA, Goergen CJ, Segers P, Vlachos PP. Color-Doppler Echocardiography Flow Field Velocity Reconstruction Using a Streamfunction -Vorticity Formulation. eprint arXiv:1812.10580 2018:arXiv:1812.10580.